Journal of Power Sources 266 (2014) 51–59

Contents lists available at ScienceDirect

Journal of Power Sources

journal homepage: www.elsevier.com/locate/jpowsour

A new model for thermal contact resistance between fuel cell gas diffusion layers and bipolar plates

Hamidreza Sadeghifar [a,b], Ned Djilali [b,c], Majid Bahrami [a,*]

[a] Laboratory for Alternative Energy Conversion (LAEC), School of Mechatronic Systems Engineering, Simon Fraser University, Surrey V3T 0A3, BC, Canada
[b] Institute for Integrated Energy Systems, University of Victoria, Victoria V8W 3P6, BC, Canada
[c] Department of Mechanical Engineering, University of Victoria, Victoria V8W 3P6, BC, Canada

HIGHLIGHTS

- Optical images show that GDL fibers are wavy and not straight.
- Thermal contact resistance (TCR) decreases with fiber wavelength.
- TCR increases with curvature, diameter and amplitude of fiber and GDL porosity.
- TCR does not change with fiber length.
- TCR variations with geometric parameters are higher at lower compression.

GRAPHICAL ABSTRACT

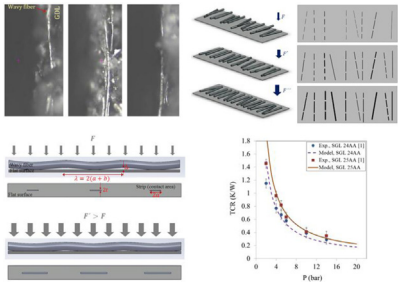

ARTICLE INFO

Article history:
Received 17 December 2013
Received in revised form
29 April 2014
Accepted 30 April 2014
Available online 15 May 2014

Keywords:
Fibrous porous media
Gas diffusion layer
Flat surface
Bipolar plate
Thermal contact resistance
Wavy Fiber

ABSTRACT

A new analytical model is developed to predict the thermal contact resistance (TCR) between fibrous porous media such as gas diffusion layers (GDLs) of polymer electrolyte membrane fuel cells (PEMFCs) and flat surfaces (bipolar plates). This robust model accounts for the salient geometrical parameters of GDLs, mechanical deformation, and thermophysical properties of the contacting bodies. The model is successfully validated against experimental data, and is used to perform in a comprehensive parametric study to investigate the effects of fiber parameters such as waviness and GDL properties on the TCR. Fiber waviness, diameter and surface curvature, as well as GDL porosity, are found to have a strong influence on TCR whereas fiber length does not affect the TCR when the porosity is kept constant. Such findings provide useful guidance for design and manufacturing of more effective GDLs for PEMFC heat management.

The analytic model can be readily implemented in simulation and modeling of PEMFCs, and can be extended with minor modifications to other fibrous porous media such as fibrous catalysts, insulating media and sintered metals.

1. Introduction

Durability, reliability and stability of polymer electrolyte membrane fuel cells (PEMFCs) are strongly dependent on heat and associated water management. It has been recently shown [1,2] that the contact resistance between the PEMFC components may be higher than their bulk resistances. However, contact resistance has typically either been roughly estimated or simply overlooked in performance model analyses [3,4]. This is mainly due to the technical barriers and challenges in measuring and predicting contact resistance, especially over a range of compression, see e.g. Refs. [5–12].

* Corresponding author. Tel.: +1 778 782 8538; fax: +1 778 782 7514.
E-mail addresses: hamidreza_sadeghifar@sfu.ca, sadeghif@sfu.ca (H. Sadeghifar), ndjilali@uvic.ca (N. Djilali), mbahrami@sfu.ca (M. Bahrami).

http://dx.doi.org/10.1016/j.jpowsour.2014.04.149
0378-7753/

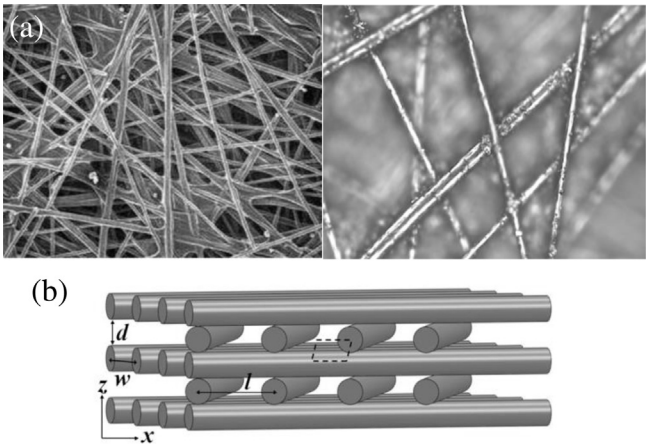

Fig. 1. (a) GDL surface images (Sigracet GDLs) and (b) Proposed geometrical modeling for a GDL.

Among the interfacial resistances in PEMFCs, the contact resistance between gas diffusion layer (GDL) and neighboring bipolar plate (BPP) is of special interest due to the rib/channel structure of the BPP compressing the adjacent GDL. The complexity of the GDL micro-structure and its surface morphology have lead most researchers to adopt numerical [13,14] and experimental [15–21] methods rather than analytic models. In our previous works (Sadeghifar et al. [1,2,5]), the thermal contact resistances (TCR) of different GDLs with metallic surfaces and also with graphite BPP were measured. The results showed that the contact resistance can be as high as the GDL bulk resistance, even for thick GDLs with thermal conductivities as low as 0.2 W m^{-1} K^{-1}. A few numerical studies have also been performed to estimate the GDL-BPP contact resistance. Using ANSYS Fluent, Nitta et al. [16] numerically estimated the contact resistance between a GDL and a graphite plate, but reported, inconsistently with contact mechanics considerations and available experimental observations, that the GDL thermal conductivity is independent of compression.

The objective of this study is to develop a mechanistic analytic model for predicting the thermal contact resistance between a GDL—a fibrous porous material—and a flat surface, e.g. a graphite or metallic BPP. The present model is built using: i) GDL and BPP salient geometric parameters, such as waviness, diameter, distribution and orientation of fibers, GDL porosity; ii) applied load, mechanical deformation, Hertzian theory; iii) thermophysical properties of both contacting bodies, i.e., fibrous porous medium and flat plate, properties such as thermal conductivities and effective Young's modulus; and iv) heat conduction in GDL fibres (spreading/constriction resistances).

2. Model development

The real area between the two contacting bodies is the key parameter in determining both electrical and thermal contact resistance. The contact area can be determined using geometrical and mechanical modeling. The TCR at the interface between a fibrous porous medium and a solid flat plate can be obtained using an appropriate thermal model that includes heat transfer in both contacting bodies through the contacting areas. This section provides an overview of different elements of the model.

2.1. Geometrical model

Based on images of different GDLs, the fibers are assumed to have a circular cross-section, as was the case in our previous works [1,8], see Fig. 1. In almost all previous GDL geometric models, the fibers are assumed to be straight, i.e. cylindrical. When modeling interfacial phenomena, which are highly dependent on surface topography and morphology, more realistic assumptions are required. Our analysis of GDL images reveals that fibers are in fact wavy, as can be seen in Fig. 2. Consequently, fibers are considered as wavy cylinders, with a sinusoidal profile in this study, see Fig. 3. The waviness of the fibers is measured optically using a mechanical tester microscope (NANOVEA). This instrument allows micro-scale imaging/filming while scanning the sample in different directions. The statistical data for fiber waviness and amplitude are presented in Fig. 4(a) and (b) for Sigracet (SGL) GDLs. The wavelength (λ) and amplitude (Δ) data fall in the ranges 50–1900 μm and 2-5d_f for the Sigracet samples. For most engineering applications, however, using the average values of fiber amplitude and wavelength may lead to sufficient accuracy.

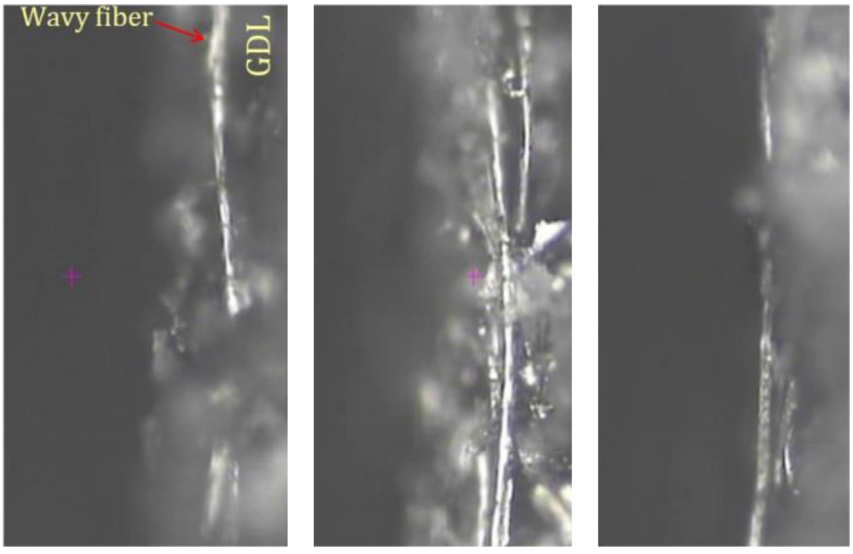

Fig. 2. GDL images showing waviness of the fibers.

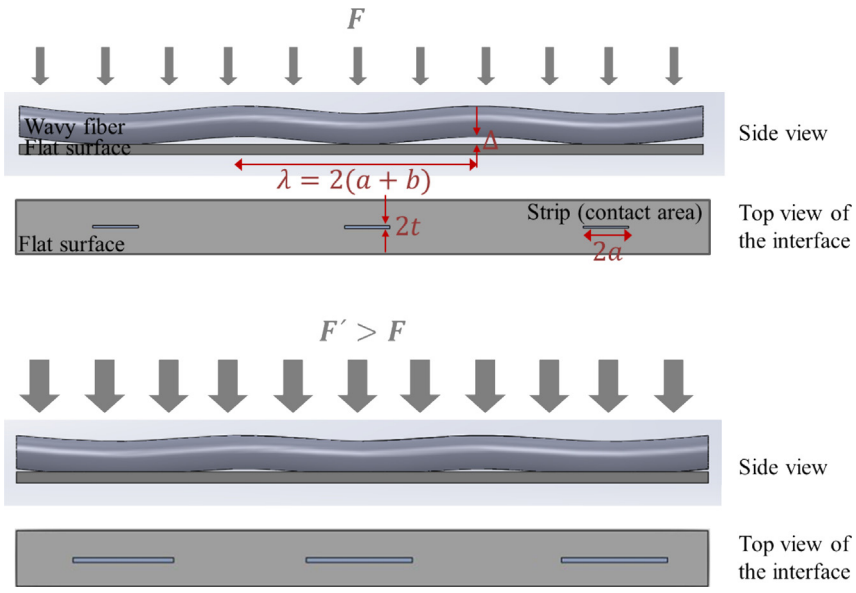

Fig. 3. A wavy fiber under compression: increasing contact areas between a wavy fiber and flat surface with increasing compression.

The proposed model is developed based on the following assumptions: 1) steady state heat transfer, 2) constant thermophysical properties, 3) wavy GDL fibers, 4) smooth flat surface, i.e., the surface roughness of the plate is neglected, 5) no out-of-flatness on the plate, 6) static mechanical contact, i.e., no vibration effects, 7) negligible radiation effects due to low typical operating temperature range of PEMFC <100 °C [1,2], and 8) first loading cycle only, i.e. no hysteresis effect is considered; but the proposed methodology is also applicable to deformed (cycled) GDLs if the deformed samples geometric parameters are available, and 9) contact occurs in a vacuum environment. It should be noted that the effects of heat transfer in interstitial gases can be added to the present model using the model of Ref. [6].

The apparent lengths of the GDL fibers were optically measured and their lengths were obtained by calculating the length of the sinusoidal arc. Nevertheless, because of the small waviness, the real length can be simply calculated mathematically:

$$l_f = 2(N_s - 1)\sqrt{\Delta^2 + \lambda^2/4} \approx l_{\text{fap}} \tag{1}$$

The total number of fibers in one layer of GDL, N_{ft}, and the number of contact strips that each fiber can form on the flat surface, N_s, can also be obtained from the geometrical data of the GDL:

$$N_{\text{ft}} = \frac{4A(1-\varepsilon)}{\pi d_f l_f} \tag{2}$$

$$N_s = \frac{L_{\text{fap}}}{\lambda} + 1 \tag{3}$$

The geometrical equations and GDLs parameters required in the model are presented in detail in Refs. [1,4,8] and are simply summarized in Table 1.

Fig. 3 shows the 'contact strips' in the contact plane, where the contact area between the flat surface and the wavy fibrous porous medium occurs. The GDL fibers have a relatively small amplitude Δ and a wavelength λ. The dimensions of these contact strips, a and t, grow with increasing compression as illustrated in Fig. 3. The contact strips dimensions can be calculated using the Hertzian contact theory and by applying a force balance. Here we first focus on the contact between one fiber and a flat surface and, then, extend the model to all contacting fibers.

2.2. Mechanical model

Thermal energy transfers from one fiber to the flat surface through the contact strips at the interface. The resistance to heat conduction depends on the contact area. The pressure distribution can be calculated for an elastic flat surface in contact with an elastic wavy cylinder, as shown in Fig. 3, from Ref. [30]:

$$p(x) = \frac{2\bar{p}\cos\left(\frac{\pi x}{\lambda}\right)}{\sin^2\left(\frac{\pi a}{\lambda}\right)}\left(\sin^2\left(\frac{\pi a}{\lambda}\right) - \sin^2\left(\frac{\pi x}{\lambda}\right)\right)^{1/2} \tag{4}$$

where x is a space variable defined along the cylinder axis and $\bar{p}$ is the mean pressure, which is related to the length of each contact strip using Hertzian theory as:

$$\bar{p} = \left(\frac{\pi E^* \Delta}{\lambda}\right)\sin^2\left(\frac{\pi a}{\lambda}\right) \tag{5a}$$

Or in an explicit form in terms of contact strip length [30]:

$$2a = \frac{2\lambda}{\pi}\arcsin\left(\frac{\lambda\bar{p}}{\pi E^* \Delta}\right) \tag{5b}$$

Using both Hertzian theory and force balances on fibers contacting the flat surface, the width of each contact strip, $2t$, can be obtained as a function of the apparent load F (the load applied on the entire GDL, see Figs. 3 and 5):

$$2t = \left(\frac{4Fd_f}{N_f(N_s - 1)aE^*\pi}\right)^{\frac{1}{2}} \tag{6}$$

It is evident from the above equations that the geometrical parameters of the contact strips are highly nonlinear and coupled, and hence no explicit functionality can be derived for the contact area dimensions. However, for most applications, the value of a/λ is small, and the term $\sin(\pi a/\lambda)$ reduces to $\pi a/\lambda$, which makes the

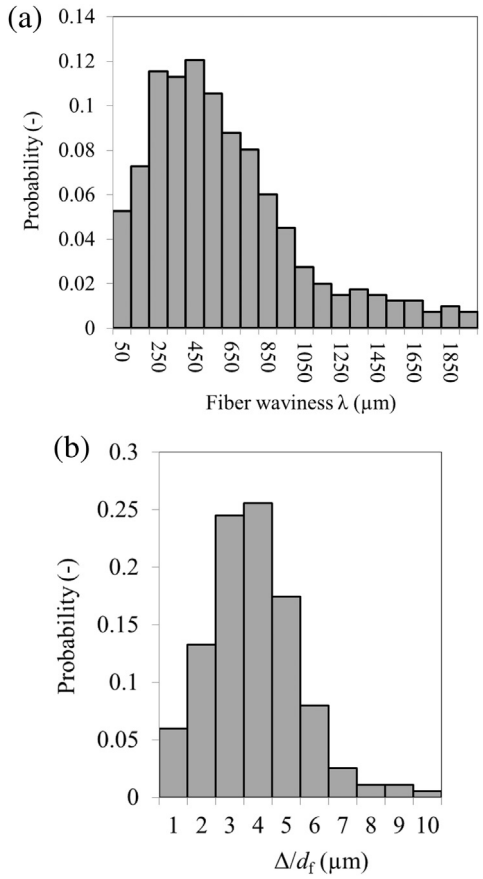

Fig. 4. Statistical data of (a) fiber waviness and (b) fiber amplitude for Sigracet (SGL) GDLs.

analysis simpler. Hence, for most applications including GDLs, one can obtain the length of each contact strip ($2a$) in terms of accessible/measurable parameters (especially F), directly from the following equation:

$$2a = \frac{1}{8\pi^4}\left(\frac{\lambda^2}{\pi\Delta}\right)^{\frac{2}{3}}\left(\frac{2F}{N_f(N_s-1)E^* d_f}\right)^{\frac{1}{3}} \tag{7}$$

Having calculated the contact strip length ($2a$), the value of the strip width ($2t$) can be directly obtained from Eq. (6).

GDL surfaces are not flat and show a random distribution of the surface asperities. Following Mikic [24] and Bahrami et al. [22], we here assume a Gaussian distribution for the distance between fibers and the flat surface, which is a function of compression as shown schematically in Fig. 5. Mikic [24] reported a relationship for the number of Gaussian asperities of an elastic body contacting a flat surface, as a function of compression, as:

$$n_s = \frac{1}{16}\left(\frac{m}{\sigma}\right)^2 \frac{\exp(-2\gamma^2)}{\mathrm{erfc}(\gamma)} A \tag{8a}$$

$$\gamma = \mathrm{erfc}^{-1}\left(\frac{4P}{H_{el}}\right) \tag{8b}$$

where m, σ, γ, A, H_{el}, P are asperity slope, GDL effective surface roughness, dimensionless mean plane separation, apparent (total) area, elastic micro-hardness, and pressure, respectively, see also Table 1. It is worth mentioning that m is a weak function of σ (see Table 1) and, for most applications, a value of $m = 0.1$ can be used [22]. The number of fibers contacting the surface (N_f) at any compression of P can be obtained by the same proportionality as Eq. (8) proposes:

$$\frac{N_f}{N_{ft}} = \frac{n_s}{n_{st}} \tag{9}$$

where N_{ft} is the total number of fibers as given in Table 1. According to Eq. (9), the present model uses only the proportionality of Eq. (8), as it obtains N_{ft} from the GDL porosity. Hence, the TCR results are not sensitive to the overall GDL roughness with a range of $1–3d_f$ reported in the literature [18,31,32].

2.3. Thermal model

Due to the very small area of the contact strips, the heat transferred from one fiber to the flat surface encounters a large resistance, mostly referred to as spreading/constriction resistance [1,8]. The spreading/constriction resistance that occurs on the cylinder (fiber) side can be obtained by Ref. [33]:

Table 1
Summary of geometrical and mechanical parameters of the studied GDLs and mechanical variables used in the present model.

Symbol	Parameter	Units	Value or equation	Basis	Eq./Fig. number
E	Young modulus of fiber & plate	GPa	210 & 210 [1,7,8]	Meas.	–
υ	Poisson ratio of fiber & plate	–	0.3 & 0.3 [1,7,8]	Meas.	–
k	Thermal conductivity of fiber & plate	W m^{-1} K^{-1}	120 & 70 [1,4,7,8]	Meas.	–
l_{fap}	Apparent fiber length	μm	3000	Meas.	–
d_f	Fiber diameter	μm	7.5 [1,8]	Meas.	–
λ	Wavelength	μm	50–1900	Meas.	Fig.4(a)
Δ	Amplitude	μm	$4d_f$	Meas.	Fig.4(b)
A	GDL cross-sectional area (apparent surface area)	m^2	0.000507 [1,8]	Meas.	–
ε	Nominal porosities of SGL 24AA & 25AA	–	0.88 & 0.92 [1,8]	Meas.	–
σ	Roughness of GDLs SGL 24AA & 25AA	m	17.0 ± 3.5 & 31.0 ± 4.5 [18,1]	Meas.	–
m	Asperities slope for GDL	–	$0.076\sigma^{0.52}$ [22–29]	Calc.	–
H_{el}	Effective elastic modulus	Pa	$\frac{E^* m}{\sqrt{2}}$ [22–24]	Calc.	–

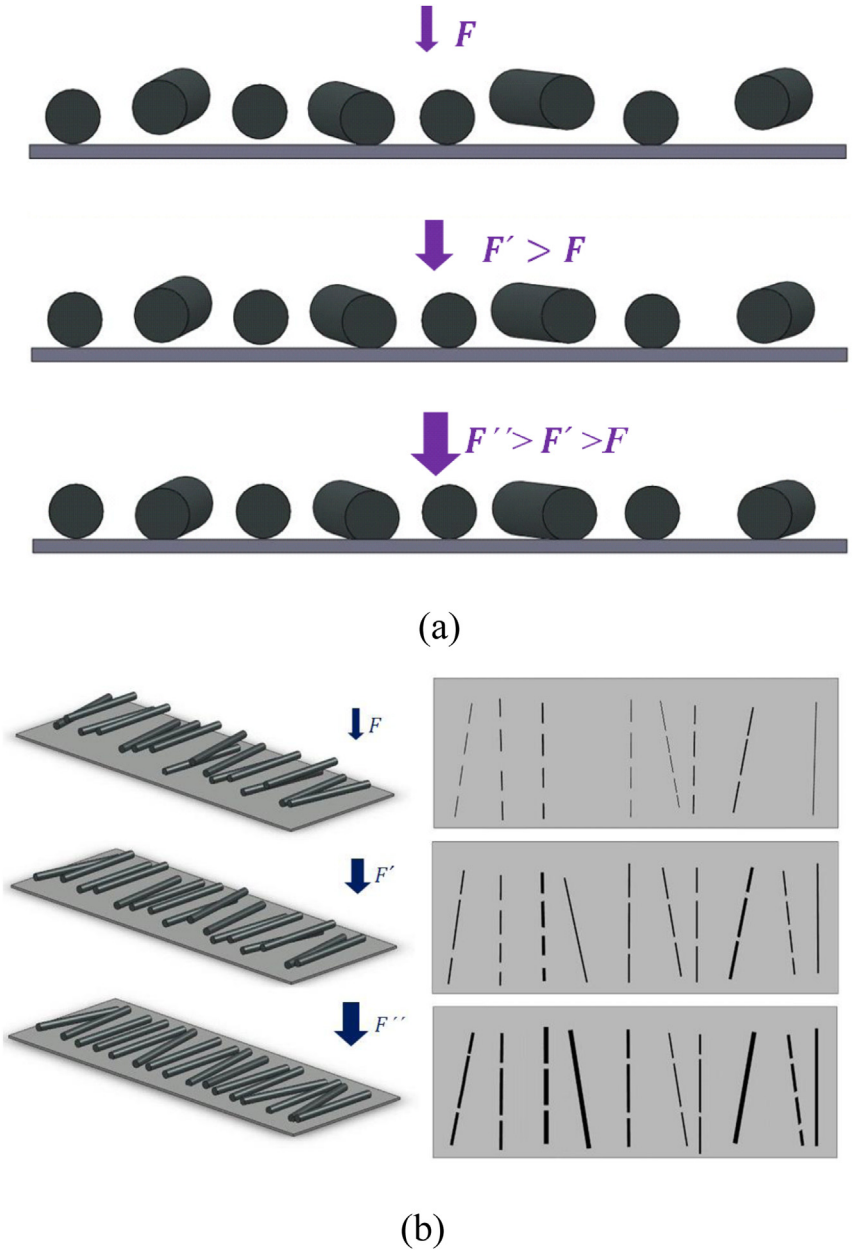

Fig. 5. (a) Gaussian distribution of the fibers at the GDL *surface* and (b) the variations in the number and size of contact areas with respect to compression ($F'' > F' > F$).

$$R_c = \frac{1}{2a\pi k_c}\ln\left(\frac{2d_f}{t}\right) - \frac{1}{4ak_c} \tag{10}$$

And that on the flat surface is given as [33]:

$$R_F = \frac{1}{a^2 u\lambda k_F}\sum_{n=1}^{\infty}\frac{\sin^2\left(\frac{2n\pi a}{\lambda}\right)}{\left(\frac{2n\pi}{\lambda}\right)^3} + \frac{1}{t^2 u\lambda k_F}\sum_{n=1}^{\infty}\frac{\sin^2\left(\frac{n\pi t}{u}\right)}{\left(\frac{n\pi}{u}\right)^3} + \frac{2}{a^2 t^2 u\lambda k_F}\sum_{n=1}^{\infty}\sum_{n=1}^{\infty}\frac{\sin^2\left(\frac{2n\pi a}{\lambda}\right)\sin^2\left(\frac{n\pi t}{u}\right)}{\left(\frac{2n\pi}{\lambda}\right)^2\left(\frac{n\pi}{u}\right)^2\sqrt{\left(\frac{2n\pi}{\lambda}\right)^2+\left(\frac{n\pi}{u}\right)^2}} \tag{11}$$

where u is the half width of the rectangular heat channels on which the isoflux (rectangular) contact strips are located centrally, which can be obtained by:

$$2u = \frac{A}{\lambda N_f(N_s - 1)} \tag{12}$$

It is worth mentioning that the summation of all the heat channels on the flat surface should be equal to the GDL cross-sectional area. A detailed explanations on the heat channel concept for contact resistance estimation can be found elsewhere [22,33].

The TCR for each contact strip is the sum of the two resistances given by Eqs. (10) and (11). Ultimately, the TCR between the GDL and the flat surface can be obtained using a parallel summation of all the contact strip resistances:

$$\mathrm{TCR} = \frac{R_C + R_F}{N_f(N_s - 1)} \tag{13}$$

The TCR averaged over all the fiber waviness can be obtained by the summation of the TCRs for different waviness based on their occurrence probability for the GDL of interest:

$$TCR_{ave\ \lambda} = \sum_{j=1}^{n_j} p_{\lambda j} TCR_{\lambda j} \quad (14)$$

where $p_{\lambda j}$ is the probability of having the waviness of λj, which is given in Fig. 4a, and $TCR_{\lambda j}$ is the value of TCR obtained from Eq. (13) for fiber waviness of λj. It should be noted that since the majority of the fiber amplitudes usually lies within a narrow range, using an average value of the amplitude is appropriate for the TCR calculations.

3. Results and discussion

Once the geometrical parameters of a GDL are determined, one can calculate the associated TCR as a function of compression. A computer code is developed in MATLAB to facilitate the TCR = f(P, λ, Δ, ε, d_f, d_{fsc}, l_f) calculations for the parametric study. It should be noted that fiber specifications (λ, Δ, d_f, d_{fsc}, l_f) and porosity (ε) of the virgin GDLs are geometric parameters required as input for the model and are hence used in the parametric study. The effect of these parameters on TCR is accounted for in conjunction with compression. For instance, with increasing compression, the number of fibers contacting the plate and the contact area dimensions (a and t) increase, as explained in Section "Mechanical model" and shown schematically in Figs. 3 and 5. The wavelength however does not change. It should be noted that all the TCR calculations in this study are based on one-inch circular GDLs ($A = 0.000507\ m^2$). The TCR per unit area of a GDL (TCR_A) can be obtained as $TCR_A = TCR \times A$.

3.1. Model validation

Fig. 6 compares the results of the present model with our experimental data [1] for two GDLs SGL 24AA and SGL 25AA. The results, shown by solid lines, are in good agreement with the experimental data and the model captures the experimental TCRs over a wide range of compression. Fig. 6 shows that the TCR decreases with increasing compression, but the slope becomes shallower and eventually, at high compression, the impact of compression on TCR becomes negligible, as expected. For SGL GDLs having an average amplitude of $\Delta/d_f = 4$ (Fig. 4b), the model is in good agreement with experiments, except for very low pressures (2 bar) where the model provided less accurate estimations of the TCR at the complex interface of the GDL-plate.

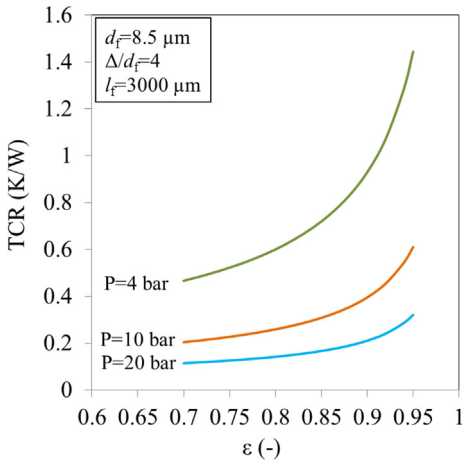

Fig. 7. Impact of porosity on the TCR at different compressions.

3.2. Parametric study

In order to investigate the effects of key parameters on the GDL-BPP TCR, a parametric study is performed in this section. For each case study, when a parameter is changed, the other parameters are kept constant unless otherwise mentioned.

3.2.1. GDL porosity (ε)

The most important and experimentally accessible parameter of a porous medium is porosity, whose effect on all the transport properties is usually significant. The effect of porosity on the TCR is shown in Fig. 7 for three compressions of 4, 10 and 20 bar. The curves show similar trends for all three compressions and with increasing porosity, the TCR increases as well. One important point is that for each curve, especially at lower compressions, there is a specific value of the porosity at which a noticeable increase can be observed at the *rate* of the TCR variations. This specific porosity, determined here at the average slope of each TCR-ε curve on Fig. 7,

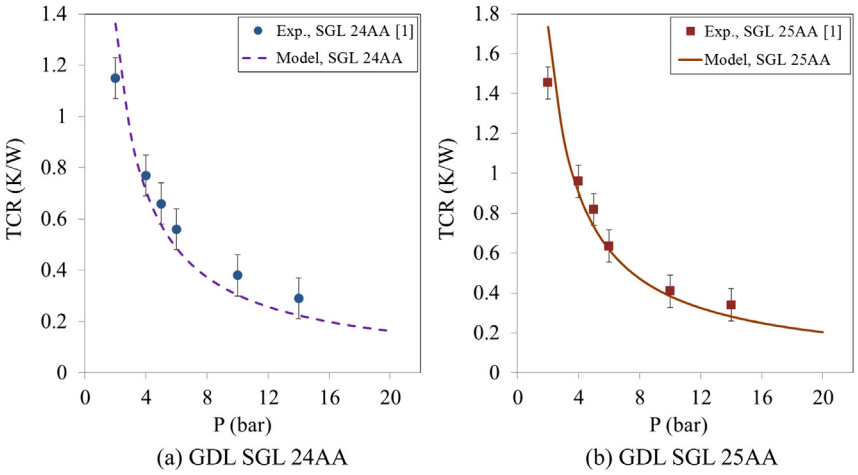

Fig. 6. Comparison of model results (solid lines) and experimental data for SGL 24AA and 25AA (the GDL specifications has already been given in Fig. 4 and Table 1: $d_f = 7.5$ μm [1,8], $l_f = 3000$ μm, $\Delta/d_f = 4$, $A = 0.000507\ m^2$ [1,8], $\varepsilon = 88.3$ & 92.1% for the GDLs SGL 24AA & 25AA, respectively).

is approximately 89% at all three compressions. This point should be accounted for in GDL manufacturing and fuel cell design.

3.2.2. Fiber length (l_f)

Fig. 8 shows that the fiber length does not have any effect on the TCR at different constant porosities. This is due to a trade-off between the number of fibers (N_f) and the number of contact strips each fiber can form on the surface (N_s) at a constant porosity. Increasing fiber lengths at constant porosity is equivalent to decreasing the number of fibers; however, the number of contact strips increases as well, so that the total number of strips remains constant throughout the interface. As a result, the contact area does not change with changing average fiber length at a constant porosity, as observed in Fig. 8.

3.2.3. Fiber wavelength (λ)

One of the two key parameters in determining the GDL-BPP TCR is the fiber wavelength and amplitude, which determines the degree of waviness that the GDL fibers have. The impact of fiber wavelength is presented in Fig. 9 for high and low porosity. TCR decreases noticeably with increasing fiber wavelength with a slope that is much more pronounced for lower compression ($P = 4$ bar) and shorter wavelengths. The rate at which the TCR decreases become markedly lower where λ reaches a specific wavelength, determined at the average slope of any of the TCR curves in Fig. 9, and corresponds approximately to 600 and 700 μm for the low and high porosity cases, respectively. This point can be an important consideration from the viewpoint of GDL manufacturing.

3.2.4. Fiber amplitude (Δ)

Fig. 10 shows that the fibre amplitude can have a strong effect on TCR. However, for typical fiber amplitudes, i.e., 3-4d_f, the effect on TCR is not significant. At larger amplitudes, especially higher than 3d_f, this effect becomes negligible at medium to high compression. A similar trend was already seen in Fig. 9 regarding the effect of the fiber wavelength on TCR.

Comparing the results of zero amplitude ($\Delta = 0$ μm), which corresponds to straight fibers, with those of other amplitudes clearly shows that the fibers waviness can increase the TCR drastically, even though its effect on the TCR drops noticeably beyond a specific value of approximately 1.5d_f. This point should be taken into account in design of both GDLs and fuel cell stacks in terms of heat management. For instance, GDLs consisting of very wavy fibers are expected to have a large contact resistance with the neighboring BPP and, hence, may be less effective in PEMFCs in terms of heat (and electrical) management.

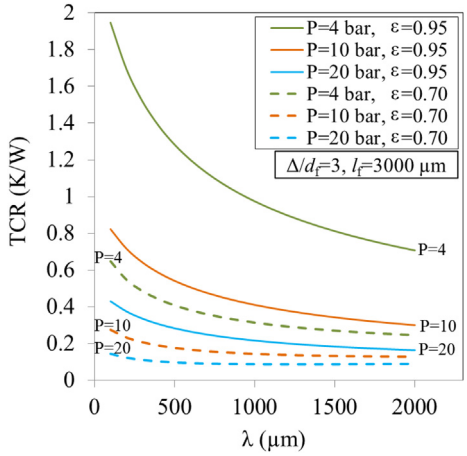

Fig. 9. Impact of fiber wavelength on the TCR for two low and high porosities at three different compressions.

3.2.5. Fiber diameter (d_f)

Fig. 11 shows that fiber diameter can significantly change the GDL-BPP TCR at low contact pressures and with increasing compression, its effect decreases. At high compressions, for a typical range of GDL fiber diameter, i.e., 7–10 μm [1,8], the effect of fiber diameter on TCR becomes insignificant.

It is worth noting that the functionality of the TCR with fiber diameter is practically linear and, hence, no critical value for fiber diameter can be determined with respect to the TCR. However, as Fig. 11 shows, with smaller fiber diameters, the TCR decreases and, eventually, converges to a very low value of 0.025 K W^{-1}, independent of the compression. This strongly suggests that GDL manufacturers explore production of GDLs with thinner fibers as long as other factors such as manufacturing capabilities or GDL mechanical strength allow.

3.2.6. Fiber surface curvature at the contact interface (d_{fsc})

Some types of fibers are not completely cylindrical; e.g., they may be ellipsoidal, while having the *same volume* as a cylindrical fiber. The deviation from a perfectly cylindrical shape can be

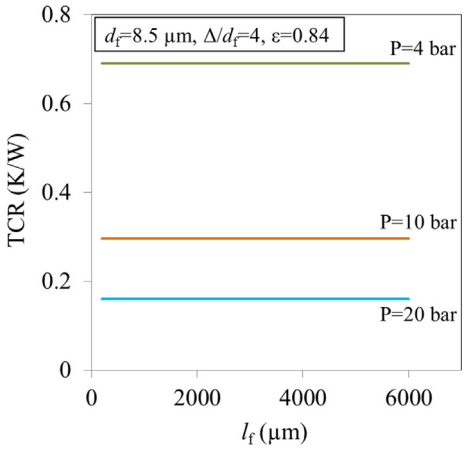

Fig. 8. Effect of fiber length on the TCR at three compressions of 4, 10 and 20 bar.

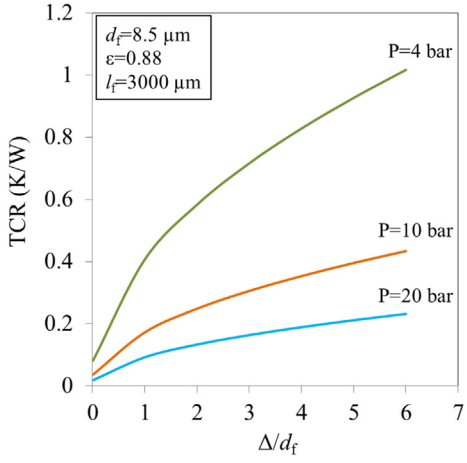

Fig. 10. Effect of amplitude on the TCR for three different compressions.

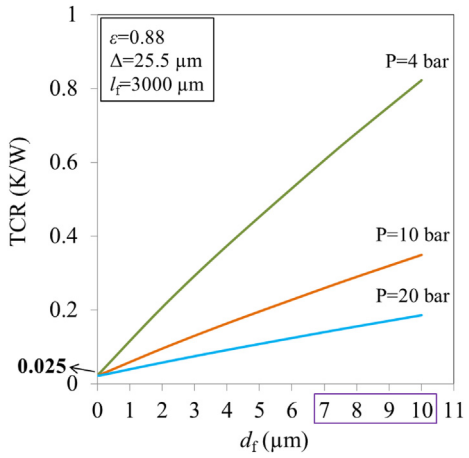

Fig. 11. Effect of fiber diameter on TCR at three compressions of 4, 10, and 14 bar: Due to almost linear functionality of TCR with fiber diameter, no critical value for fiber diameter can be determined. However, the TCR reduces to 0.025 K W^{-1} as fiber diameter approaches zero (all the other parameters except for the number of fibers are kept constant to keep the GDL porosity unchanged ($\varepsilon = 0.88$)).

accounted for by considering the effect of fiber surface curvature at the contact interface. The effect on TCR of fiber curvature (which in the limit of a cylinder is the fiber diameter) can be analyzed without changing any parameters to keep the GDL porosity constant (e.g., without changing the number of fibers). Fig. 12 shows that, whereas TCR varies linearly with fiber diameter, its dependence on fiber surface curvature is highly non-linear and is particularly significant at very small curvatures. Comparing Figs. 11 and 12 also shows that, for typical values of fiber diameter and fiber curvature, the TCR is not as sensitive to the fiber surface curvature as to the fiber diameter (which determines both fiber surface curvature and fiber volume). Overall, the points presented in this study can also be taken into account in determining the TCR of GDLs with catalyst coated membranes (CCMs) [34] and microporous layers (MPLs) [35].

4. Summary and conclusion

A new and robust mechanistic model was developed for predicting the thermal contact resistance between a general fibrous medium and a flat surface, and was applied to analyze the contact between PEMFC gas diffusion layers and bipolar plates. The model accounts for the salient geometrical parameters, mechanical deformation and thermophysical properties, and captures accurately experimentally-observed behavior over a wide range of compression, except for very low compression (less than ~2 bar) where the model provided rough predictions of the TCR.

The model allows systematic investigation of the impact of the main GDL micro structural properties on TCR without having to rely entirely on more difficult experimental measurements. The simple and general model developed in this study can be readily implemented into fuel cell models and may also be used for modeling the behavior of any other fibrous porous materials such as fibrous insulations.

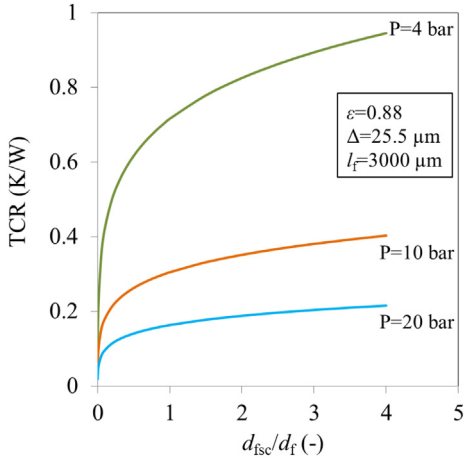

Fig. 12. Effect of fiber surface curvature at the contact interface on the TCR: $d_f = d_{fsc}$ in all the equations except for Eq. (2) which relates the GDL porosity with the number and volume of the fibers.

Acknowledgment

The authors gratefully acknowledge the financial support of the Natural Sciences and Engineering Research Council of Canada (NSERC). The authors also appreciate SGL Carbon Company, especiallyNico Haak and Susanne Bacher, for providing the samples andalso for some technical guidance regarding the SGL GDLsspecifications.

References

[1] H. Sadeghifar, N. Djilali, M. Bahrami, J. Power Sources 248 (2014) 632–641.
[2] H. Sadeghifar, N. Djilali, M. Bahrami, J. Power Sources (2014) (revision).
[3] H. Sadeghifar, M. Bahrami, N. Djilali, in: ASME 10th Fuel Cell Science, Engineering and Technology Conference, July 23–26, 2012. San Diego, CA, USA, Paper No. ESFuelCell2012-91160.
[4] N. Zamel, Xi Li, J. Shen, J. Becker, A. Wiegmann, Chem. Eng. Sci. 65 (2010) 3994–4006.
[5] H. Sadeghifar, M. Bahrami, Thermal Conductivity of Ballard's Graphite Bipolar Plates, Ballard Technical Report, No. BPP-0926–1012/1, Laboratory for Alternative Energy Conversion, Simon Fraser University, Vancouver, BC, Canada, September 2012.
[6] M. Bahrami, M.M. Yovanovich, J.R. Culham, J. Thermophys. Heat Transf. 18 (2004) 326–332.
[7] E. Sadeghi, M. Bahrami, N. Djilali, J. Power Sources 179 (2008) 200–208.
[8] H. Sadeghifar, M. Bahrami, N. Djilali, J. Power Sources 233 (2013) 369–379.
[9] E. Sadeghi, N. Djilali, M. Bahrami, J. Power Sources 196 (2011) 246–254.
[10] E. Sadeghi, N. Djilali, M. Bahrami, J. Power Sources 195 (2010) 8104–8109.
[11] E. Sadeghi, N. Djilali, M. Bahrami, J. Power Sources 196 (2011) 3565–3571.
[12] M.F. Mathias, J. Roth, J. Fleming, W. Lehnert, Diffusion media materials and characterisation, in: W. Vielstich, H.A. Gasteiger, A. Lamm (Eds.), Handbook of Fuel Cells: Fundamentals, Technology and Applications, John Wiley, New York, 2003.
[13] J. Becker, V. Schulz, A. Wiegmann, J. Fuel Cell Sci. Technol. 5 (2008) 21006–21015.
[14] M. Wang, J. He, J. Yu, N. Pan, Int. J. Therm. Sci. 46 (2007) 848–855.
[15] H. Sadeghifar, V. Norouzifard, M. Bahrami, Bulk and Interfacial Transport Properties of Porous Fuel Cell Materials, AFCC-NSERC CRD Grant Proposal, Vancouver, BC, Canada, 2014.
[16] I. Nitta, O. Himanen, M. Mikkola, Fuel Cells 08 (2008) 111–119.
[17] O. Burheim, P.J.S. Vi, J.G. Pharoah, S. Kjelstrup, J. Power Sources 195 (2010) 249–256.
[18] A. El-kharouf, T.J. Mason, Dan J.L. Brett, B.G. Pollet, J. Power Sources 218 (2012) 393–404.
[19] H. Sadeghifar, M. Bahrami, N. Djilali, in: ASME 11th Fuel Cell Science, Engineering and Technology Conference, July 14–19, 2013. Minneapolis, MN, USA, Paper No. ES-FuelCell2013-18072.
[20] H. Sadeghifar, M. Bahrami, Thermal and Electrical Resistances of Mercedes Benz Fuel Cell Samples: Effects of Compression, Temperature, Load Cycling, and Assembly, Mercedes Benz Fuel Cell (MBFC) Technical Report, No. MEAGDLCCM-1030–1113/1, Laboratory for Alternative Energy Conversion, Simon Fraser University, Vancouver, BC, Canada, October 2013.
[21] H. Sadeghifar, M. Bahrami, N. Djilali, Thermal conductivity of Sigracet gas diffusion layers and MPL: part I, in: Effect of Compression, PTFE, MPL, Cyclic Load and Hysteresis Behavior, Hydrogen & Fuel Cell Conference, June 16–19, 2013. Vancouver, BC, Canada.
[22] M. Bahrami, Modeling of Thermal Joint Resistance for Rough Sphere-flat Contact in a Vacuum, PhD Thesis, University of Waterloo, Spring 2004.
[23] M. Bahrami, J.R. Culham, M.M. Yovanovich, G.E. Schneider, ASME J. Appl. Mech. Rev. 59 (2006) 1–12.
[24] B.B. Mikic, Int. J. Heat Mass Transf. 17 (1974) 205–214.

[25] M. Bahrami, M.M. Yovanovich, J.R. Culham, Int. J. Heat Mass Transf. 49 (2006) 3691–3701.
[26] M. Bahrami, M.M. Yovanovich, J.R. Culham, ASME J. Trib. 127 (2005) 884–889.
[27] M. Bahrami, M.M. Yovanovich, J.R. Culham, AIAA J. Thermophys. Heat Transf. 18 (2004) 326–332.
[28] M. Bahrami, J.R. Culham, M.M. Yovanovich, ASME J. Heat Transf. 126 (6) (2004) 896–905.
[29] M. Bahrami, M.M. Yovanovich, J.R. Culham, AIAA J. Thermophys. Heat Transf. 21 (2007) 153–157.
[30] K.L. Johnson, Contact Mechanics, Cambridge University Press, UK, 1985.
[31] C. Leising, Fuel Cell Gas Diffusion Layer Inspection with 3D Profilometry, Today's Standard for Tomorrow's Materials, NANOVEA Company, CA, USA, 2010. http://www.nanovea.com.
[32] Toray Carbon Paper, http://www.fuelcellstore.com.
[33] M.M. Yovanovich, E.E. Marotta, Thermal Spreading and Contact Resistance, 2003. Chapter 4.
[34] H. Sadeghifar, N. Djilali, M. Bahrami, A Novel Approach to Measuring in-plane Electrical Conductivity of a Catalyst Coated Membrane (CCM) and its Electrical Contact Resistance with Fuel Cell Gas Diffusion Layers (GDLs) and Micro Porous Layers (MPLs): Effect of Compression, PTFE and Humidity, 2014, 97th Canadian Chemistry Conference and Exhibition, Vancouver, BC, Canada.
[35] H. Sadeghifar, N. Djilali, M. Bahrami, Role of Micro Porous Layer (MPL) in Electrical and Thermal Resistances of Fuel Cell Gas Diffusion Layers (GDLs), 2014, 97th Canadian Chemistry Conference and Exhibition, Vancouver, BC, Canada.

Nomenclature

A: GDL cross-sectional area, m^2
a: half of contact strip length, m
b: length of non-contacting area, $b = \lambda/2 - a$, m
Calc.: based on calculation or derivation
d_f: fiber diameter, m
d_{fsc}: diameter of fiber surface curvature at the contact interface, m
E: Young (elastic) modulus, Pa
E^*: $= (1 - \nu_C^2/E_C + 1 - \nu_F^2/E_F)$ Effective Young (elastic) modulus, Pa
Exp.: experimental value
F: force applied on the entire GDL, N
GDL: gas diffusion layer
k: thermal conductivity, W m^{-1} K^{-1}
l_f: fiber length, m
l_{fap}: apparent fiber length, m
Meas.: based on measurement
N_f: number of fibers contacting the surface at the pressure of P
N_{ft}: total number of fibers contacting the surface
N_s: number of troughs (strips) each fiber has (forms on the flat surface)
n_s: number of asperities contacting the surface of another body in contact
n_{st}: total number of asperities contacting the surface
P: pressure on the entire GDL, Pa
$\overline{p}$: mean pressure, Pa
PEMFC: polymer electrolyte membrane fuel cell
R: thermal resistance, K W^{-1}
R_c: spreading/constriction resistance on cylinder side resistance, K W^{-1}
R_F: spreading/constriction resistance on flat surface side, K W^{-1}
t: half of strip width, m
TCR: thermal contact resistance, K W^{-1}
TCR_A: specific-area TCR: Thermal contact resistance per unit area (=TCR × A), K W^{-1} m^2
u: half of the width of the rectangular channel area, m
x: a space variable defined along the cylinder axis

Greek letter

Δ: amplitude of fiber waviness, m
γ: non-dimentional separation
ε: porosity
λ: wavelength of fiber waviness, m
σ: root mean square (RMS) roughness of GDL (=d_f for the parametric study), m
υ: Poisson's ratio

Subscript

C: cylinder
f: fiber
F: flat surface
m: measured
n: summation index
t: total value